

# Neutrino-pair emission from nuclear de-excitation in core-collapse supernova simulations

T. Fischer,<sup>1</sup> K. Langanke,<sup>2,3,4</sup> and G. Martínez-Pinedo<sup>3,2</sup>

<sup>1</sup>*Institute for Theoretical Physics, University of Wrocław, plac M. Borna 9, 50-204 Wrocław, Poland*

<sup>2</sup>*GSI Helmholtzzentrum für Schwerionenforschung, Planckstraße 1, D-64291 Darmstadt, Germany*

<sup>3</sup>*Institut für Kernphysik, Technische Universität Darmstadt, Schlossgartenstraße 2, D-64289 Darmstadt, Germany*

<sup>4</sup>*Frankfurt Institute for Advanced Studies, Ruth-Moufang Straße, D-60438 Frankfurt, Germany*

(Received 17 September 2013; published 6 December 2013)

We study the impact of neutrino-pair production from the de-excitation of highly excited heavy nuclei on core-collapse supernova simulations, following the evolution up to several 100 ms after core bounce. Our study is based on the AGILE-BOLTZTRANsupernova code, which features general relativistic radiation hydrodynamics and accurate three-flavor Boltzmann neutrino transport in spherical symmetry. In our simulations the nuclear de-excitation process is described in two different ways. At first we follow the approach proposed by Fuller and Meyer [*Astrophys. J.* **376**, 701 (1991)], which is based on strength functions derived in the framework of the nuclear Fermi-gas model of noninteracting nucleons. Second, we parametrize the allowed and forbidden strength distributions in accordance with measurements for selected nuclear ground states. We determine the de-excitation strength by applying the Brink hypothesis and detailed balance. For both approaches, we find that nuclear de-excitation has no effect on the supernova dynamics. However, we find that nuclear de-excitation is the leading source for the production of electron antineutrinos as well as heavy-lepton-flavor (anti)neutrinos during the collapse phase. At sufficiently high densities, the associated neutrino spectra are influenced by interactions with the surrounding matter, making proper simulations of neutrino transport important for the determination of the neutrino-energy loss rate. We find that, even including nuclear de-excitations, the energy loss during the collapse phase is overwhelmingly dominated by electron neutrinos produced by electron capture.

DOI: 10.1103/PhysRevC.88.065804

PACS number(s): 26.30.Jk, 97.60.Bw, 26.50.+x

## I. INTRODUCTION

Massive stars end their lives as supernovae, triggered by the collapse of their central core. It has long been recognized that neutrinos play a crucial role in the dynamics of the collapsing core [1,2] and the associated supernova nucleosynthesis [3]. Once the electron chemical potential gets sufficiently large at densities of order  $10^9 \text{ g cm}^{-3}$ , electrons are captured on protons bound in nuclei [4]. This has the following two important consequences for the collapse dynamics: it reduces the pressure which the relativistic electron gas can supply against the collapse and the (electron) neutrinos, which are produced from weak-interaction processes, leave the star carrying away energy and lepton number. In fact, this cooling mechanism keeps the core at relatively low entropies so that heavy nuclei survive the collapse and are the dominant component of the nuclear composition [5]. With increasing core density, neutrino interactions with matter become growingly more relevant. Coherent elastic neutrino scattering on nuclei [6] leads to neutrino trapping for densities in excess of about  $10^{12} \text{ g cm}^{-3}$ . Inelastic neutrino scattering on electrons, and to a lesser extent on nuclei [4], down-scatters neutrinos in energy and ultimately leads to the thermalization of the trapped neutrinos. Hence in the late stage of the collapse, i.e., at densities in excess of  $10^{12} \text{ g cm}^{-3}$ , a Fermi sea of electron neutrinos is formed in the inner core that effectively Pauli-blocks further electron capture.

In supernovae weak charged-current reactions produce electron neutrinos and antineutrinos. Other neutrino types can only be generated by processes governed by neutral currents, i.e., in the form of neutrino-antineutrino pairs. In current supernova simulations, neutrino-pair production

is considered via electron-positron annihilation, nucleon-nucleon bremsstrahlung, and the annihilation of trapped electron-neutrino and antineutrino pairs into heavy-lepton-flavor neutrino-antineutrino pairs [7]. It has been argued that the de-excitation of highly excited nuclei can be the dominant neutrino-pair-producing process in the hot environment of the collapsing core [8] [for an illustration, see Fig. 1(a)]. As the presence of the electron neutrino sea does not block the production of muon and tau neutrino-antineutrino pairs nor that of electron antineutrinos, simultaneously produced in a pair with a high-energy electron neutrino, nuclear de-excitation might further reduce the entropy of the collapsing core if the neutrinos produced by the process can leave the core during the dynamical time scale of the collapse. Indeed if the produced neutrinos have energies low enough to leave the stellar core, it is speculated that the de-excitation process “likely acts as a thermostat for the collapsing core”; i.e., in a self-regulating process more escaping neutrinos are being produced the hotter the core temperature [8].

In this manuscript, we report on supernova simulations that include the nuclear de-excitation processes. To this end we evolve an  $11.2M_{\odot}$  star [3] from the presupernova progenitor through the core collapse, bounce, and post-bounce evolution for more than 300 ms. Our study is based on the AGILE-BOLTZTRAN supernova code (see Ref. [9] and references therein for additional details).

In nuclear de-excitation a highly excited state at energy  $E_i$  decays via  $Z^0$  emission to a final state at lower energy  $E_f$  [for illustration, see Fig. 1(a)]. The energy difference,  $\Delta = E_i - E_f$ , between the nuclear states is shared by the  $\nu\bar{\nu}$  pair which is created by the decay of the  $Z^0$  boson. [The situation is

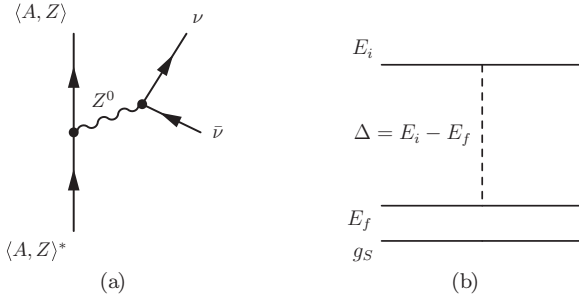


FIG. 1. (a) Feynman diagram for the de-excitation of a heavy nucleus via the emission of a neutrino pair. (b) Schematic diagram for the situation of an excited heavy nucleus with excitation energy  $E_i$  decaying to a state of lower energy  $E_f$ , above the ground state  $g_s$ . The quantity  $\Delta$  is the energy difference between initial and final states.

illustrated in Fig. 1(b).] For small values of  $\Delta$ , the total nuclear strength is dominated by Gamow-Teller (GT) transitions. At higher energy differences  $\Delta$ , forbidden transitions will contribute. Modeling such transitions for an ensemble of thermally excited nuclear states at moderate temperatures ( $T \approx 1\text{--}2$  MeV) typical for a supernova environment is a challenging problem. It cannot be solved by current models for the relevant heavy nuclei, due to the extremely high density of states involved. As a first approach, rates for nuclear excitation and de-excitation have been estimated on the basis of the nuclear Fermi gas model, i.e., describing the nucleus as an ensemble of noninteracting nucleons occupying a set of shell-model orbits [8]. The rates for up-transitions, i.e., the nuclear excitation via the absorption of a neutrino pair, obtained in this model have been recently qualitatively supported based on the interacting shell model [10]. As our first scheme to describe the de-excitation process in a supernova simulation, we have adopted the respective rates of Ref. [8] and have incorporated them into the supernova AGILE-BOLTZTRAN code.

To study the sensitivity of the supernova results on potential uncertainties in the de-excitation rates we describe the latter also within an alternative approach. Here we start from the observation that the relevant Gamow-Teller (and forbidden) strength is constrained experimentally for selected nuclear ground states, showing that the various strengths is mainly concentrated in strong transitions (the GT and spin-dipole giant resonances). Adopting Brink's hypothesis [11], in which the transition strengths on excited nuclear states are assumed to be the same as for the ground state, and exploiting the principle of detailed balance allows us to derive the “downward” transition strengths required for modeling the de-excitation rate from experimentally motivated parametrization of the Gamow-Teller and forbidden ground-state strengths.

The paper is organized as follows. In Sec. II we review our core-collapse supernova model, and in Sec. III we discuss the implementation of new rates for electron capture on heavy nuclei as well as the neutrino-pair production from nuclear de-excitation. In Sec. IV, we apply these new weak rates in core-collapse simulations and discuss the results. We close the manuscript with a summary in Sec. V.

TABLE I. Neutrino reactions considered.

	Weak process <sup>a</sup>	References
1	$e^- + p \rightleftharpoons n + \nu_e$	[13]
2	$e^+ + n \rightleftharpoons p + \bar{\nu}_e$	[13]
3	$e^- + (A, Z) \rightleftharpoons (A, Z-1) + \nu_e$	[14]
4	$\nu + N \rightleftharpoons \nu' + N$	[12,15]
5	$\nu + (A, Z) \rightleftharpoons \nu' + (A, Z)$	[12,15]
6	$\nu + e^\pm \rightleftharpoons \nu' + e^\pm$	[12,16]
7	$e^- + e^+ \rightleftharpoons \nu + \bar{\nu}$	[12]
8	$N + N \rightleftharpoons \nu + \bar{\nu} + N + N$	[17]

<sup>a</sup>Note:  $\nu = \{\nu_e, \bar{\nu}_e, \nu_{\mu/\tau}, \bar{\nu}_{\mu/\tau}\}$  and  $N = \{n, p\}$ .

## II. CORE-COLLAPSE SUPERNOVA MODEL

Our core-collapse supernova code, AGILE-BOLTZTRAN, is based on general relativistic radiation hydrodynamics and three-flavor Boltzmann neutrino transport in spherical symmetry (for details, see Ref. [9] and references therein). The set of weak processes that we consider in our supernova simulations (including the references which we have used) are listed in Table I. The charged-current processes (1) and (2) as well as the elastic scattering reaction (4) are important in regions where the composition is dominated by nucleons. The charged-current reactions with nucleons are treated in the zero-momentum transfer approximation [12,13]. Electron-positron annihilation (7) dominates the production of neutrino pairs at low and intermediate densities, while nucleon-nucleon bremsstrahlung becomes important at higher densities, around a tenth of normal nuclear matter density. We also include the annihilation of trapped electron-neutrino pairs [process (9) in Table I]. Inelastic neutrino scattering on electrons and positrons, reaction (6) in Table I, is the dominant thermalization process for neutrinos [4].

At the high-density environment of a core-collapse supernova, electron neutrinos are more strongly coupled to matter by process (1) than are electron antineutrinos by process (2) (see Table I). Hence, electron antineutrinos decouple at generally higher densities than electron neutrinos. Moreover, heavy-lepton neutrinos do not interact by charged-current processes at the relevant conditions and are hence even less coupled to matter than electron antineutrinos; they decouple from matter at even higher densities. Consequently, during the post-bounce mass accretion phase when matter at neutrino decoupling is extremely neutron rich, the following hierarchy holds for the average neutrino energies:  $\langle E_{\nu_{\mu/\tau}} \rangle \gtrsim \langle E_{\nu_e} \rangle > \langle E_{\bar{\nu}_e} \rangle$  [18–20].

The equation of state (EoS) in core-collapse supernova studies has to handle a variety of conditions that relate to different nuclear regimes. It spans from isospin-symmetric matter at low densities and temperatures dominated by heavy nuclei up to supersaturation densities where matter is extremely neutron rich and temperatures reach several tens of MeV. AGILE-BOLTZTRAN uses a flexible EoS module that allows for the use of a large variety of currently available supernova equations of state [21–23]. For a comparison study of different supernova equation of states, see Refs. [24,25]. For the current study, we apply the EoS from Ref. [21] with compressibility  $K = 220$  MeV for matter at temperatures above  $T = 0.45$  MeV.

The baryon EoS is then computed based on the ideal gas approximation. In addition to the baryons, contributions from electrons, positrons, and photons are added [26].

### III. WEAK PROCESSES WITH HEAVY NUCLEI

#### A. Electron capture on heavy nuclei

Compared to previous studies performed with the AGILE-BOLTZTRAN code we have improved the description of electron capture by implementing the reaction rates for electron captures on nuclei [process (3) in Table I] as derived in Ref. [14]. The authors of Ref. [14] determined their rate tabulation from individual capture rates for about 3000 nuclei, valid for matter in nuclear statistical equilibrium (NSE). To derive the individual rates the authors adopted a hierarchy of nuclear models to ensure the appropriate description of the electron capture process at all conditions of the collapse. In particular, the capture rate for nuclei in the mass range  $A = 45\text{--}64$  was derived on the basis of the interacting shell model. It guarantees an accurate and detailed description of the allowed strength distribution [27] required to describe the electron capture rate at the moderate density conditions at which these medium-mass nuclei dominate. The capture rate for heavier nuclei with  $A = 65\text{--}120$  were derived within the framework of the random phase approximation (RPA) with partial nuclear occupation numbers obtained in large-scale shell-model Monte Carlo (SMMC) calculations at finite temperature [28–30]. These two data sets have been supplemented by individual rates for more than 2000 additional nuclei using an SMMC + RPA approach, similar to the one introduced in Ref. [31] but with parametrized occupation numbers.

The authors of Ref. [14] provide a table for the electron-capture rates and neutrino spectra for a fixed three-dimensional grid in temperature  $T$ , electron fraction  $Y_e$ , and density  $\rho$ , valid for NSE above  $T > 0.45$  MeV. We apply a linear interpolation scheme in these three variables to determine the rates and spectra for the appropriate astrophysical conditions.

#### B. Neutrino-antineutrino pair emission and absorption

Emission and absorption of neutrino pairs is a process that can potentially affect the dynamics of the core. In this section we derive expressions for the rate of heavy-nuclei de-excitation and excitation that can be used in core-collapse supernova simulations. The decay rate of a nucleus from a state with excitation energy  $E_1$  via emission of neutrino-antineutrino pairs of a particular flavor is given by [8]

$$\begin{aligned} \lambda_{\nu\bar{\nu}}(E_1) = & \frac{2\pi}{\hbar} \frac{G_F^2 g_A^2 (4\pi)^2}{(2\pi\hbar c)^6} \int_0^{E_1} dE_2 \int_0^{\Delta} E_{\bar{\nu}}^2 E_\nu^2 dE_\nu \frac{1}{(4\pi)^2} \\ & \times \int_{-1}^{+1} d\mu_\nu \int_{-1}^{+1} d\mu_{\bar{\nu}} [1 - f_\nu(E_\nu, \mu_\nu)] \\ & \times [1 - f_{\bar{\nu}}(E_{\bar{\nu}}, \mu_{\bar{\nu}})] \int_0^{2\pi} d\phi_\nu \\ & \times \int_0^{2\pi} d\phi_{\bar{\nu}} S^{\text{down}}(E_1, \Delta, \cos\theta), \end{aligned} \quad (1)$$

where

$$\Delta = E_1 - E_2 = E_\nu + E_{\bar{\nu}}, \quad (2)$$

and where  $G_F$  is the Fermi coupling constant and  $g_A$  the weak axial-vector coupling constant. We account for the presence of neutrinos by including the neutrino and antineutrino distribution functions  $f_\nu(E_\nu, \mu_\nu)$  that, due to our assumption of spherical symmetry, depend only on the radius, energy, and the cosine of the angle with respect to the radial direction,  $\mu_\nu$ , and not on the azimuthal angle,  $\varphi_\nu$ .  $S^{\text{down}}(E_1, \Delta, \cos\theta)$  is the strength function connecting a state with excitation energy  $E_1$  to a state with excitation energy  $E_2 = E_1 - \Delta$  and  $\theta$  is the angle between the emitted neutrino-antineutrino pair that is related to the neutrino angles by

$$\cos\theta = \mu_\nu \mu_{\bar{\nu}} + \sqrt{(1 - \mu_\nu^2)(1 - \mu_{\bar{\nu}}^2)} \cos\phi (\phi = \varphi_\nu - \varphi_{\bar{\nu}}). \quad (3)$$

The first integral of Eq. (1) represents the contributions of all the different states to which the excited state can decay. Furthermore, we have included a factor of  $(4\pi)^2$  in front of the integrals that represents the value of the angular integrals assuming isotropicity. Here, we follow the standard convection in nuclear  $\beta$  decay. We can perform a change of variables, using Eq. (2), so that the integrals are performed as a function of the neutrino and antineutrino energies:

$$\begin{aligned} \lambda_{\nu\bar{\nu}}(E_1) = & \lambda_0 \int_0^{E_1} dE_\nu \int_{-1}^{+1} d\mu_\nu E_\nu^2 [1 - f_\nu(E_\nu, \mu_\nu)] \\ & \times \int_0^{E_1 - E_\nu} dE_{\bar{\nu}} \int_{-1}^{+1} d\mu_{\bar{\nu}} E_{\bar{\nu}}^2 [1 - f_{\bar{\nu}}(E_{\bar{\nu}}, \mu_{\bar{\nu}})] \\ & \times \frac{1}{(4\pi)^2} \int_0^{2\pi} d\phi_\nu \\ & \times \int_0^{2\pi} d\phi_{\bar{\nu}} S^{\text{down}}(E_1, E_\nu + E_{\bar{\nu}}, \cos\theta), \end{aligned} \quad (4)$$

where

$$\lambda_0 = \frac{G_F^2 g_A^2}{2\pi^3 \hbar (\hbar c)^6}. \quad (5)$$

In order to obtain the total rate of neutrino-pair production from heavy-nuclei de-excitations, all possible transitions have to be included properly weighted by the appropriate Boltzmann factor and the level-density,  $\rho(E, J)$ . One then obtains

$$\lambda_{\nu\bar{\nu}} = \frac{1}{Z(T)} \int_0^\infty dE (2J + 1) \rho(E, J) \lambda_{\nu\bar{\nu}}(E) e^{-E/T} \quad (6)$$

with  $Z(T) = \int dE (2J + 1) \rho(E, J) e^{-E/T}$ , the partition function. Using Eq. (4) and after changing the integration order we obtain

$$\begin{aligned} \lambda_{\nu\bar{\nu}} = & \lambda_0 \int_0^\infty dE_\nu \int_{-1}^{+1} d\mu_\nu E_\nu^2 [1 - f_\nu(E_\nu, \mu_\nu)] \\ & \times \int_0^\infty dE_{\bar{\nu}} \int_{-1}^{+1} d\mu_{\bar{\nu}} E_{\bar{\nu}}^2 [1 - f_{\bar{\nu}}(E_{\bar{\nu}}, \mu_{\bar{\nu}})] \\ & \times \frac{1}{(4\pi)^2} \int_0^{2\pi} d\phi_\nu \int_0^{2\pi} d\phi_{\bar{\nu}} S^{\text{emi}}(T, E_\nu + E_{\bar{\nu}}, \cos\theta), \end{aligned} \quad (7)$$

where we have introduced the thermal strength function for emission of a neutrino-antineutrino pair:

$$\begin{aligned} \mathcal{S}^{\text{emi}}(T, E_\nu + E_{\bar{\nu}}, \cos \theta) &= \frac{1}{Z(T)} \int_0^\infty dE (2J+1) \rho(E, J) \\ &\times S^{\text{down}}(E, E_\nu + E_{\bar{\nu}}, \cos \theta) e^{-E/T}. \end{aligned} \quad (8)$$

The strength function, which connects states 1 and 2 ( $S^{\text{down}}$ ) with the energy relation  $E_1 = E_2 + \Delta$ , is associated with the strength function connecting states 2 and 1 ( $S^{\text{up}}$ ) by detailed balance [32–34]:

$$\begin{aligned} &(2J_1+1)\rho(E_1, J_1)S^{\text{down}}(E_1, \Delta, \cos \theta) \\ &= (2J_2+1)\rho(E_2, J_2)S^{\text{up}}(E_2, \Delta, \cos \theta). \end{aligned} \quad (9)$$

Note that the above expression is commonly used to relate the down and up  $\gamma$ -ray strength functions in the calculation of radioactive capture reactions [35]. We obtain the following relationship between the thermal strength functions for emission and absorption of a pair of neutrinos:

$$\begin{aligned} \mathcal{S}^{\text{emi}}(T, E_\nu + E_{\bar{\nu}}, \cos \theta) &= \mathcal{S}^{\text{abs}}(T, E_\nu + E_{\bar{\nu}}, \cos \theta) \\ &\times \exp\left(-\frac{E_\nu + E_{\bar{\nu}}}{T}\right), \end{aligned} \quad (10)$$

where  $\mathcal{S}^{\text{abs}}$  is related to  $S^{\text{up}}$  by an equation similar to Eq. (8).

The total number of neutrino pairs produced per unit of volume and time,  $\Lambda_{\nu\bar{\nu}}$ , is given by the decay rate for nuclear species  $i$ , called  $\lambda_{\nu\bar{\nu}}^i$ , weighted with the total number density of nuclei  $n_i$  and summing over all nuclear species present in the medium,

$$\Lambda_{\nu\bar{\nu}} = \sum_i n_i \lambda_{\nu\bar{\nu}}^i. \quad (11)$$

In the Boltzmann representation of neutrino transport this quantity is normally described by the pair-emission kernel,  $R^{\text{emi}}(E_\nu + E_{\bar{\nu}}, \cos \theta)$ . The total rate for  $\nu\bar{\nu}$  emission, based on the reaction kernel  $R^{\text{emi}}$ , has the general form

$$\begin{aligned} \Lambda_{\nu\bar{\nu}} &= \frac{1}{(2\pi\hbar c)^6} \int_0^\infty dE_\nu E_\nu^2 \int_{-1}^{+1} d\mu_\nu [1 - f_\nu(E_\nu, \mu_\nu)] \\ &\times \int_0^\infty dE_{\bar{\nu}} E_{\bar{\nu}}^2 \int_{-1}^{+1} d\mu_{\bar{\nu}} [1 - f_{\bar{\nu}}(E_{\bar{\nu}}, \mu_{\bar{\nu}})] \\ &\times \int_0^{2\pi} d\varphi_\nu \int_0^{2\pi} d\varphi_{\bar{\nu}} R^{\text{emi}}(E_\nu + E_{\bar{\nu}}, \cos \theta). \end{aligned} \quad (12)$$

Comparing this expression with Eq. (7), we obtain

$$R^{\text{emi}}(\Delta, \cos \theta) = \frac{2\pi}{\hbar} G_F^2 g_A^2 \sum_i n_i \mathcal{S}_i^{\text{emi}}(T, \Delta, \cos \theta). \quad (13)$$

The absorption kernel is related to absorption strength by a similar expression. As a consequence of Eq. (10), we obtain the general detailed balance expression for the kernel [12]:

$$\begin{aligned} R^{\text{emi}}(E_\nu + E_{\bar{\nu}}, \cos \theta) &= R^{\text{abs}}(E_\nu + E_{\bar{\nu}}, \cos \theta) \\ &\times \exp\left(-\frac{E_\nu + E_{\bar{\nu}}}{T}\right). \end{aligned} \quad (14)$$

Finally, the de-excitation process is considered in the Boltzmann transport equation [12,20,36] by adding an appropriate

contribution to the source term:

$$\begin{aligned} B_{\text{NDE}}[f_\nu] &= \frac{1}{c(2\pi\hbar c)^3} \left\{ [1 - f_\nu(E_\nu, \mu_\nu)] \int_0^\infty dE_{\bar{\nu}} E_{\bar{\nu}}^2 \right. \\ &\times \int_{-1}^{+1} d\mu_{\bar{\nu}} [1 - f_{\bar{\nu}}(E_{\bar{\nu}}, \mu_{\bar{\nu}})] \\ &\times \int_0^{2\pi} d\varphi_{\bar{\nu}} R^{\text{emi}}(E_\nu + E_{\bar{\nu}}, \cos \theta) \\ &- f_\nu(E_\nu, \mu_\nu) \int_0^\infty dE_{\bar{\nu}} E_{\bar{\nu}}^2 \int_{-1}^{+1} d\mu_{\bar{\nu}} f_{\bar{\nu}}(E_{\bar{\nu}}, \mu_{\bar{\nu}}) \\ &\left. \times \int_0^{2\pi} d\varphi_{\bar{\nu}} R^{\text{abs}}(E_\nu + E_{\bar{\nu}}, \cos \theta) \right\}, \end{aligned} \quad (15)$$

with a similar equation for  $f_{\bar{\nu}}$ , i.e.,  $f_\nu \leftrightarrow f_{\bar{\nu}}$ . For the particular case in which neutrinos escape freely from the stellar core we can define the total (including all neutrino flavors) nuclear de-excitation rate as

$$\lambda = \frac{3G_F^2 g_A^2}{60\pi^3 \hbar (\hbar c)^6} \int_0^\infty E^5 \bar{\mathcal{S}}^{\text{emi}}(T, E) dE. \quad (16)$$

The factor of 3 accounts for the three possible neutrino flavors that can be produced in the decay and we have used the fact that the strength function depends only on the sum of neutrino energies to perform one of the energy integrations in Eq. (7). We have also introduced the angle-averaged thermal strength function

$$\begin{aligned} \bar{\mathcal{S}}(T, E) &= \frac{1}{(4\pi)^2} \int_{-1}^{+1} d\mu_\nu \int_0^{2\pi} d\varphi_\nu \int_{-1}^{+1} d\mu_{\bar{\nu}} \\ &\times \int_0^{2\pi} d\varphi_{\bar{\nu}} \mathcal{S}(T, E, \cos \theta). \end{aligned} \quad (17)$$

Equivalently, we can define the de-excitation energy loss rate as

$$\dot{Q} = \frac{3G_F^2 g_A^2}{60\pi^3 \hbar (\hbar c)^6} \int_0^\infty E^6 \bar{\mathcal{S}}^{\text{emi}}(T, E) dE. \quad (18)$$

We can also define the neutrino (antineutrino) spectra, i.e., the number of neutrinos per energy and time, produced by nuclear de-excitations by integrating over the antineutrino (neutrino) energy as follows:

$$\mathcal{N}_\nu(E) = \frac{G_F^2 g_A^2}{2\pi^3 \hbar (\hbar c)^6} E^2 \int_0^\infty dE_{\bar{\nu}} E_{\bar{\nu}}^2 \bar{\mathcal{S}}^{\text{emi}}(T, E_\nu + E_{\bar{\nu}}). \quad (19)$$

### C. Strength function

To determine the neutrino-pair de-excitation rate we have to determine the temperature, neutrino-pair energy, and angle dependence of the thermal strength function  $\mathcal{S}(T, E, \cos \theta)$  [see Eq. (8)]. As the process is expected to be relevant at temperatures around 1 MeV and higher, correspondingly at nuclear excitation energies above  $\sim 10$  MeV, a state by state evaluation of the total rate is prohibited due to the overwhelmingly large density of levels involved. Hence one has to turn to an “averaged” way in describing the respective strength function. Here we will follow two alternative approaches.

In the first approach we follow the proposal of Fuller and Meyer [8] in which analytical expressions for the emission and absorption thermal strength functions using a Fermi gas model were developed. The parameters were adjusted to reproduce the results obtained in an independent single-particle shell model. Fuller and Meyer considered a strength distribution that consists of both allowed and first-forbidden contributions and assumed different angular dependence for each of them:

$$S(T, E, \cos \theta) = S_A(T, E)P_A(\cos \theta) + S_F(T, E)P_F(\cos \theta). \quad (20)$$

We refer to the work of Fuller and Meyer [8] for the particular form of the strength functions,  $S_A$  and  $S_F$ , and their dependence on nuclear mass and charge,  $A$  and  $Z$ , respectively. However, we used the angular dependence of the functions  $P_A$  and  $P_F$  as

$$P_A(\cos \theta) = 1 - \frac{1}{3} \cos \theta, \quad P_F(\cos \theta) = 1, \quad (21)$$

which is differently normalized as defined by Fuller and Meyer and has been chosen such that

$$\bar{S}^{\text{emi}}(T, E) = S_A(T, E) + S_F(T, E), \quad (22)$$

which is the angle-averaged thermal strength function [see Eq. (17)]. With the angular dependence of Eq. (20), the azimuthal integral in the source term for nuclear de-excitation (NDE) can be performed to obtain

$$B_{\text{NDE}}[f_\nu] = \frac{2\pi}{c(2\pi\hbar c)^3} \left\{ [1 - f_\nu(E_\nu, \mu_\nu)] \int_0^\infty dE_{\bar{\nu}} E_{\bar{\nu}}^2 \right. \\ \times \int_{-1}^{+1} d\mu_{\bar{\nu}} [1 - f_{\bar{\nu}}(E_{\bar{\nu}}, \mu_{\bar{\nu}})] \\ \times \mathcal{R}^{\text{emi}}(E_\nu + E_{\bar{\nu}}, \mu_\nu, \mu_{\bar{\nu}}) - f_\nu(E_\nu, \mu_\nu) \\ \times \int_0^\infty dE_{\bar{\nu}} E_{\bar{\nu}}^2 \int_{-1}^{+1} d\mu_{\bar{\nu}} f_{\bar{\nu}}(E_{\bar{\nu}}, \mu_{\bar{\nu}}) \\ \left. \times \mathcal{R}^{\text{abs}}(E_\nu + E_{\bar{\nu}}, \mu_\nu, \mu_{\bar{\nu}}) \right\}, \quad (23)$$

with

$$\mathcal{R}(E, \mu_\nu, \mu_{\bar{\nu}}) = \frac{2\pi}{\hbar} G_F^2 g_A^2 \sum_i n_i \left[ S_A^i(T, E) \left( 1 - \frac{\mu_\nu \mu_{\bar{\nu}}}{3} \right) \right. \\ \left. + S_F^i(T, E) \right]. \quad (24)$$

In a recent work, Misch *et al.* [10] have calculated allowed down strength functions for several nuclei including  $^{28}\text{Si}$ ,  $^{47}\text{Ti}$ , and  $^{56}\text{Fe}$  at different excitation energies based on the diagonalization shell model. In their study they approximate the thermal strength to the one obtained for an excitation energy equivalent to the average thermal excitation energy  $\langle E \rangle$  determined by assuming a Fermi gas model,  $\langle E \rangle = T^2 A / 8$ . This approach has two main disadvantages. First, it violates detailed balance according to Eq. (10), and more importantly for the calculation of de-excitation rates it results in a sharp cutoff in the production of neutrino pairs of energies larger than the thermal average energy. The production of these high-energy neutrinos is suppressed by the Boltzmann

factor but it is favored by the large phase space dependence [see Eq. (16)].

In the following, we propose an alternative approach which fulfills detailed balance by construction and accounts for the production of neutrinos with energies greater than the average thermal excitation. We derive the thermal strength guided by experimental knowledge of the allowed and forbidden strengths for nuclear ground states. It is well known that the allowed (Gamow-Teller) and forbidden (dipole) strength  $S^{\text{up}}$  on nuclear ground states resides mainly in giant resonances [37]. This is observed in  $(p, p')$  [38,39] (as well as in charge-exchange experiments of  $N = Z$  nuclei [40,41], which determine  $S^{\text{up}}$  due to isospin symmetry). Much information about giant resonances has been obtained from  $(e, e')$  experiments performed over the entire nuclear chart [42]. The experiments have been supplemented by theoretical studies where in particular large-scale shell-model calculations give a very fair account of the detailed structure of the allowed strength distribution [43], while studies of the forbidden strength is the domain of models like the (quasiparticle) random phase approximation [44]. The experimental and theoretical studies indicate that the allowed strength is concentrated in a giant resonance with a centroid energy at about  $E_x = 8\text{--}10$  MeV, reflecting mainly an excitation of nucleons between spin-orbit partner orbitals. As the dipole strength corresponds to a transition between two adjacent major shells, its giant resonance resides at somewhat higher excitation energies with a centroid around  $E_x = 18\text{--}24$  MeV. Both the giant Gamow-Teller and dipole resonances are strongly fragmented over many states and the strength distribution can be approximated by a Gaussian distribution around the respective centroids [45,46].

We will assume that the giant resonances built on excited states are located at the same relative excitation energy as for the ground state. This is commonly known as the Brink hypothesis and implies that the up strength at any excitation energy is equal to that of the ground state,  $S^{\text{up}}(E, \Delta) = S_{\text{gs}}^{\text{up}}(\Delta)$ . This approximation is commonly done in calculations of astrophysical reaction rates based on the statistical model [47] and implies that the thermal absorption strength becomes independent of the temperature and is given by

$$S^{\text{abs}}(T, \Delta) = S_{\text{gs}}^{\text{up}}(\Delta). \quad (25)$$

However, we note that, due to nuclear structure effects (pairing, angular momentum mismatch, etc.) and the low density of levels, the upward strengths on the ground state vanish or are strongly suppressed at low excitation energies. This behavior is not expected for the upward strength on excited states as they are populated at the temperatures of interest for the neutrino-pair de-excitation process. We account for this expectation by assuming that the strength is fragmented over a larger energy range than for the ground state, while the total strength is the same as for the ground state. Guided by these assumptions we make the following ansatz for the absorption thermal strength:

$$S^{\text{abs}}(\Delta) = S_A g(\Delta, \mu_A, \sigma_A) + S_F g(\Delta, \mu_F, \sigma_F), \quad (26)$$

where  $S_A$  and  $S_F$  are the total allowed and forbidden strength and  $g$  is the normalized strength distribution with centroid

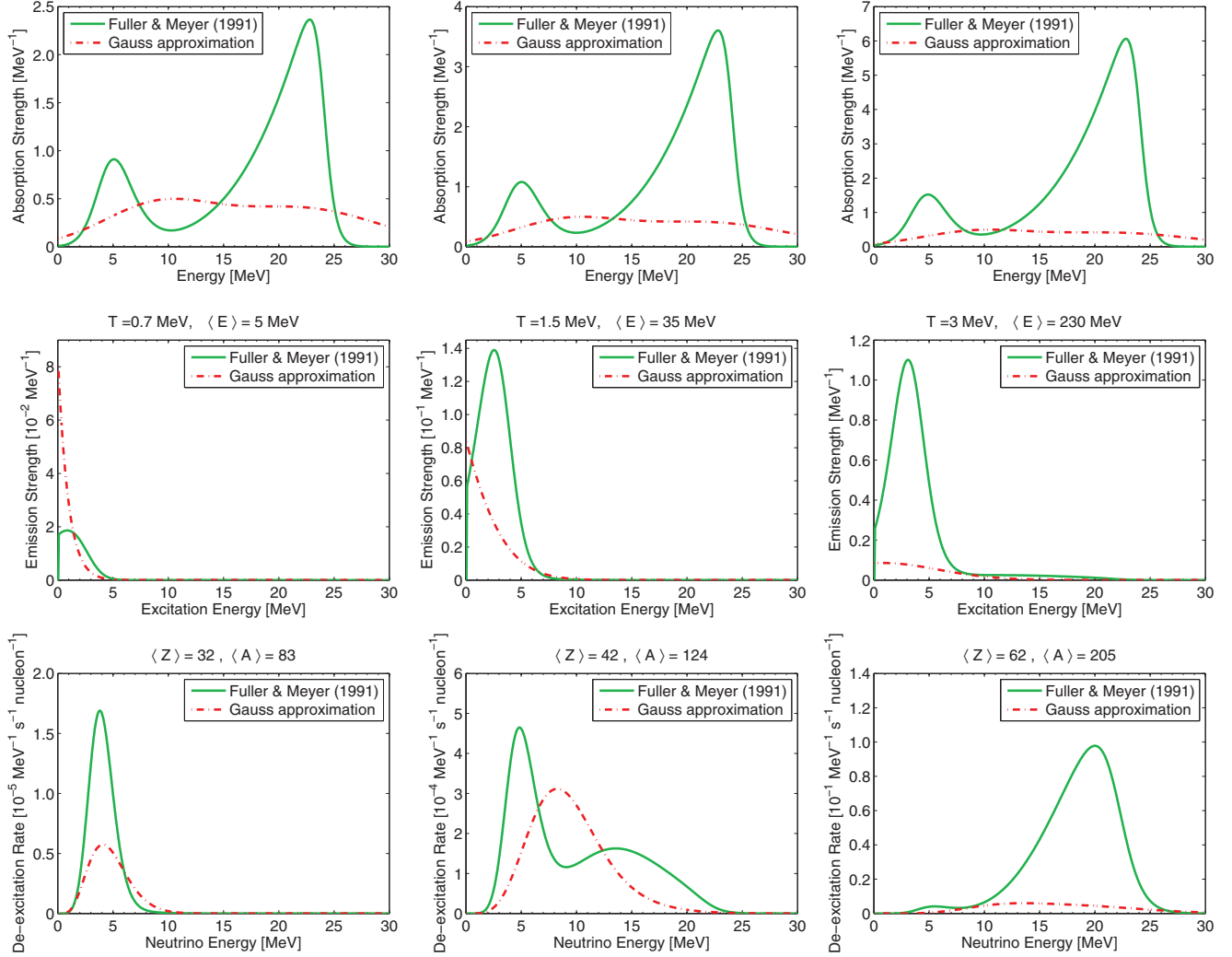


FIG. 2. (Color online) Strength for absorption (top panels) and emission (middle panels) of neutrino pairs based on the Fermi-gas model of Ref. [8] (green lines) and our approach (red lines; see text for a description) at temperatures of  $T = 0.7$  MeV (left panel),  $T = 1.5$  MeV (middle panel), and  $T = 3.0$  MeV (right panel). The corresponding conditions are listed in Table II. The bottom panels show the de-excitation rate versus energy, i.e., the integrand in Eq. (16).

$\mu$  and standard deviation  $\sigma$  that we assume to follow the Gaussian distribution. The total allowed strength,  $S_A = 5$ , is chosen in accordance with the value found for nuclei in the iron region [48–50], while the forbidden strength,  $S_F = 7$ , is chosen guided by RPA calculations [50,51]. For the centroid and standard deviation we use  $\mu_A = 9$  MeV,  $\sigma_A = 5$  MeV,  $\mu_F = 22$  MeV, and  $\sigma_F = 7$  MeV. The emission thermal strength is then obtained by applying detailed balance [see Eq. (10)]. Our ansatz should be considered as a simple approximation as it neglects a temperature dependence of the width parameters and assumes the strength to be the same for all nuclei. At low temperatures we also expect deviations from a Gaussian distribution caused by the discrete level structure for the allowed strength and the nonequilibration of parity in the level density at low energies for the forbidden strength.

The top panels of Fig. 2 compare the absorption strength function  $\mathcal{S}^{\text{abs}}$  [see Eq. (10)] for the two approaches considered in our study. We use the composition given by the EoS

at selected temperatures, densities, and  $Y_e$  values obtained from our simulations. The strength function derived by Fuller and Meyer shows rather distinct peaks for allowed and forbidden transitions, while in our ansatz the strengths for these transitions are fragmented over a wider energy range. We note that the differences become quite pronounced at low ( $E < 1$  MeV) and high ( $E > 25$  MeV) energies where the strength suggested by Fuller and Meyer basically vanishes, while the Gaussian ansatz, expression (26), shows noticeable strength. Furthermore, the Fuller and Meyer approach [8] predicts a total strength that is proportional to the number of nucleons. This explains the increase of strength with temperature, as observed in Fig. 2, as the nuclear composition moves to heavier nuclei with increasing temperature in the supernova environment. Hence the two cases considered here can be understood as extreme cases for the absorption strength.

The middle panels of Fig. 2 shows the thermal emission strength functions  $\mathcal{S}^{\text{emi}}$ , which are obtained from the thermal

absorption functions by multiplication with the Boltzmann factor  $\exp(-E/T)$ . Due to this factor the thermal emission strength strongly depends on temperature. Note that, while our absorption strength is independent of temperature and is the same for all nuclei, the one suggested by Fuller and Meyer is weakly dependent on temperature and increases with increasing nucleon number. We note that the differences in the two absorption strength functions lead to quite strong deviations in the emission functions. The emission functions derived from the Gaussian absorption function show a continuous decrease with energy, reflecting mainly the exponential decrease of the Boltzmann factor as the corresponding absorption function varies only slowly in the energy range of importance. As the absorption strength suggested by Fuller and Meyer has very little strength at vanishing energy, this energy range is also suppressed in the emission strength functions, which show a pronounced peak at moderately low energies. We note that there is also emission strength at energies above the thermal average energy (denoted by  $\langle E \rangle$  in the middle panels for each temperature), due to the thermal population of states at higher energies. However, the Boltzmann factor forces the emission strength to vanish at high energies. Obviously, the developing tails of the emission functions depend on temperature and on the assumptions on the absorption strength function.

The tails in the emission functions are more pronounced in the de-excitation rate, i.e., the integrand of Eq. (16). This quantity is shown in the bottom panels of Fig. 2. One clearly observes that the production of neutrinos with energies higher than the average nuclear excitation energy is important. In particular at low temperatures,  $T = 0.7$  MeV, where  $\langle E \rangle \sim 5$  MeV, the maximum of the pair de-excitation rate is located at higher energies than the average excitation energy. Comparing the results for the two strength function approaches at  $T = 1.5$  MeV, one finds that the Fermi-gas approximation [8] exhibits two peaks, which can be associated with the distinct allowed and forbidden transitions. At higher temperatures (see the right panel of Fig. 2), forbidden transitions even dominate the de-excitation rate. The emission strength resulting from the Gaussian strength function shows a single peak structure at all temperatures due to the rather broad strength functions used in our parametrization. However, an increasing role of forbidden strength with increasing temperature is also predicted.

#### D. Spectra comparison under supernova conditions

Figure 3 shows the (anti)neutrino spectra produced by nuclear de-excitation [as defined in Eq. (19)] and electron capture. The spectra are compared at three different stages of the collapse phase, where we have chosen the temperatures to match those adopted in Fig. 2. We note that the spectra do not include final-state Pauli blocking of the neutrinos. Hence the de-excitation spectra basically depend on temperature, with a density dependence arising for the nuclear Fermi-gas results with its  $A$ -dependent strength function due to the change of the nuclear composition. As the electron Fermi energy strongly depends on density, the neutrino spectra produced by electron capture do as well. The three conditions chosen correspond to the progenitor phase (upper panel), the stage

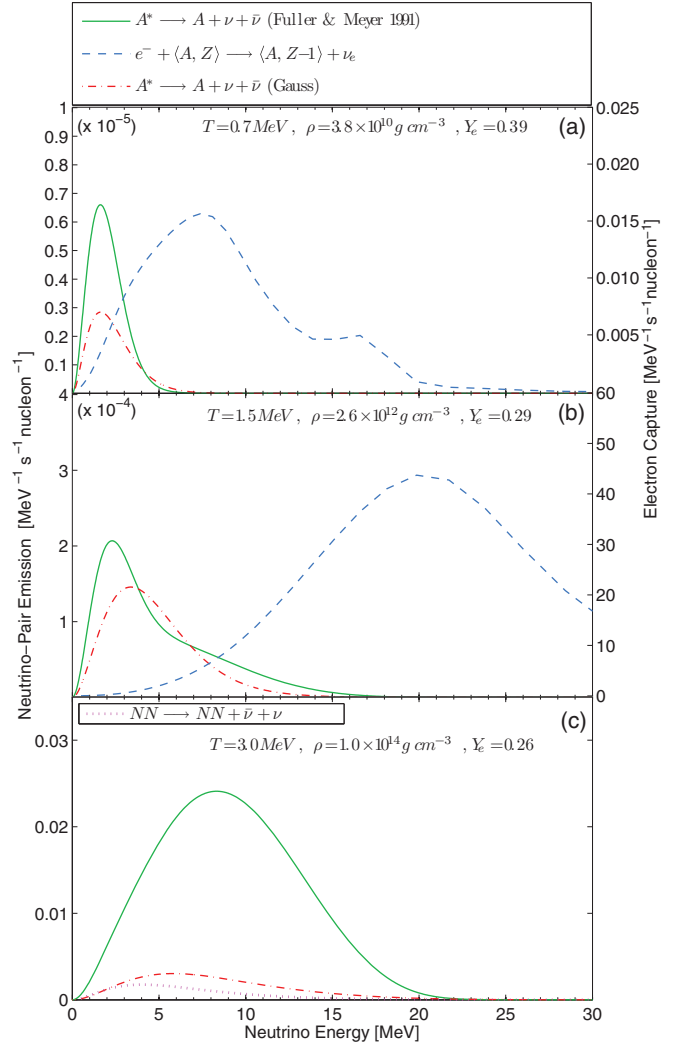


FIG. 3. (Color online) Total neutrino emission spectra, comparing electron capture on heavy nuclei [14] (red dash-dotted lines) and heavy-nuclei de-excitation based on Fuller and Meyer [8] (blue solid lines), as well as expression (26) (red dash-dotted lines), at low (a), intermediate (b), and high temperatures and densities (c), i.e., corresponding to entries in Table II. In the bottom panel, instead of electron capture we show the  $\nu\bar{\nu}$ -emission rate from  $N$ - $N$  bremsstrahlung (magenta dotted line). For the upper and middle panels the neutrino emission spectra have to be multiplied by the number shown in parentheses.

of electron neutrino trapping (middle panel), and the late phase before bounce where a transition to uniform nuclear matter is taking place. At all conditions, electron captures produce neutrino spectra with significantly higher energies. This is confirmed in Table II in which we have summarized the average neutrino energies produced by electron capture and for our two approaches to nuclear de-excitation, assuming that the produced neutrinos leave the star unhindered. To understand these results we note that for electron capture the relevant energy scale is the electron Fermi energy, which grows from about 10 to 100 MeV in the density range covered by Fig. 3 [6]. Hence this process produces on average higher-energy neutrinos than nuclear de-excitation for which

TABLE II. Average energy of the neutrino produced by electron capture and nuclear de-excitations ( $\nu\bar{\nu}$ ), for selected conditions during the collapse.

$T$ (MeV)	$\rho$ (g cm $^{-3}$ )	$Y_e$	$\langle E \rangle^{\text{ecap}}$ (MeV)	$\langle E \rangle^{\nu\bar{\nu}}$ (MeV)	
			Ref. [14]	Ref. [8]	This work
0.55	$2.0 \times 10^{10}$	0.42	8.54	1.82	1.86
0.70	$3.8 \times 10^{10}$	0.39	8.91	2.05	2.32
1.00	$4.2 \times 10^{11}$	0.33	12.08	2.57	3.27
1.50	$2.6 \times 10^{12}$	0.29	21.36	4.93	4.68
2.00	$8.5 \times 10^{12}$	0.27	27.51	7.45	5.96
3.00	$2.0 \times 10^{14}$	0.26	75.46 <sup>a</sup>	9.21	9.04

<sup>a</sup>Includes only the contribution from  $e^-$  capture on protons.

the average neutrino energies  $\langle E \rangle \propto T$  due to the dominance of the Boltzmann factor  $\exp(-E/T)$ , as explained above in connection with Fig. 2. From Fig. 3 and Table II we observe that at the lower temperatures the Fermi-gas-based model for nuclear de-excitation produces neutrinos with slightly lower average neutrino energies than our Gaussian strength model, while it is the opposite for temperatures  $T \gtrsim 1.5$  MeV. As explained above this is related to the stronger contributions of forbidden transitions in the strength function of Ref. [8].

The neutrino spectra shown in Fig. 3 are unnormalized and the most important result is obtained by comparing the scales of the two processes, electron capture and nuclear de-excitation, showing that the former exceeds the latter by about 5 orders of magnitude. This implies that electron capture will be the dominating weak-interaction process for the global properties of supernovae, while the importance of nuclear de-excitation is constrained to the results concerning neutrino types other than electron neutrinos. These expectations are confirmed in our supernova simulations, which we turn to in the following section. Note that in Fig. 3(c) we show  $N$ - $N$ bremssstrahlung, in addition to nuclear de-excitation, which starts to become important as heavy nuclei disappear at densities in excess of  $\sim 10^{13}$  g cm $^{-3}$ .

Table II lists the expected average neutrino energies from heavy-nuclei de-excitations ( $\nu\bar{\nu}$ ), under the assumption that all neutrinos produced can leave the star. At temperatures above 1.5 MeV, corresponding to densities above  $10^{12}$  g cm $^{-3}$ , the average neutrino energies become larger than 5 MeV, so that down-scattering of electrons becomes relevant, implying substantial changes for the neutrino spectra and making proper neutrino transport important. This expectation is confirmed by the results of our simulations presented in the next section.

#### IV. SIMULATION RESULTS OF STELLAR CORE COLLAPSE

In this section, we discuss results from core-collapse supernova simulations of the  $11.2M_\odot$  progenitor [3], focussing on the effects of heavy-nuclei de-excitation by neutrino-pair emission. To this end, we have performed three supernova simulations which differ only in their treatments of the neutrino-pair de-excitation process. In two simulations we include nuclear de-excitation following either the prescription of Fuller and Meyer [8] or our Gaussian approximation model.

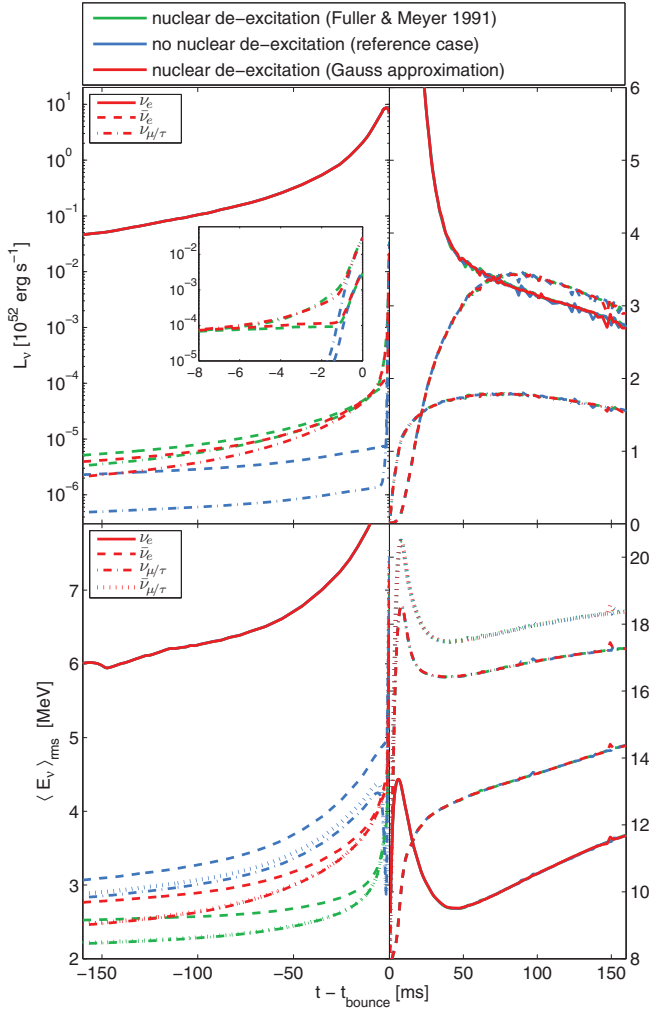


FIG. 4. (Color online) Evolution of neutrino luminosities and root-mean-square average energies from core-collapse supernova simulations for which we include the production of neutrino pairs from heavy-nuclei de-excitations, based on Ref. [8] (green lines) and the Gauss approximation expression (26) (red lines), in comparison to a simulation that uses the standard set of weak rates as listed in Table I (blue lines) and otherwise identical input physics.

The third simulation serves as a control study, in which we have switched off neutrino-pair de-excitation. We use the extended set of electron capture rates of Juodagalvis *et al.* [14] in all our simulations. We note that our control run yields results which agree quite well with those obtained in Refs. [29,30], in which a subset of the Juodagalvis capture rates (consisting of the shell model and SMMC + RPA rates of Refs. [29,52,53]) is used, indicating that the extension of the electron capture rate set has only small impact on supernova simulations. However, the control simulation leads to a noticeable lower central electron fraction due to a longer deleptonization phase before heavy nuclei dissolve and also to a different electron-fraction structure toward lower densities at core bounce than obtained in studies based on the schematic description of electron capture provided by Ref. [12].

The results of our three simulations are presented in Fig. 4 and in Figs. 5–7. Figure 4 shows the time evolution of

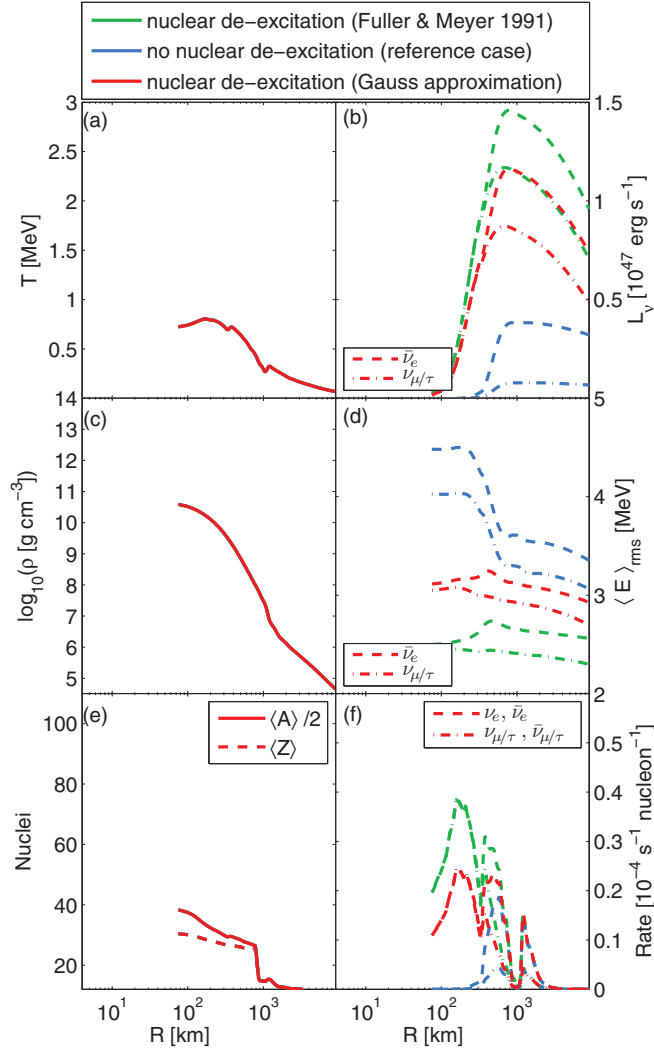


FIG. 5. (Color online) Radial profile of selected quantities at about 50 ms before core bounce, comparing simulations for which we include the production of neutrino pairs from heavy-nuclei de-excitations, based on Ref. [8] (green lines), and the Gauss approximation expression (26) (red lines), in comparison to a simulation that uses the standard set of weak rates as listed in Table I (blue lines) and otherwise identical input physics.

the neutrino luminosities (upper panel) and root-mean-square (RMS) average energies (bottom panel) for all neutrino flavors, determined at a distance of 1000 km. Note that we determine the time of core bounce arbitrarily as the moment when the maximum central density is reached; i.e., it is the moment just before shock breakout. Figures 5–7 show core profiles of various quantities before bounce.

Importantly, we find in these figures that the global quantities such as temperature and electron fraction profiles are the same in all three simulations (with differences seen in Fig. 4 being due to slight mismatches in the determination of core bounce in the different runs and due to different grid resolutions). This implies that the neutrino-pair heavy-nuclei de-excitation process has no impact on the global supernova evolution. As expected from our discussion above, the rates for electron capture on nuclei (and protons) dominate over

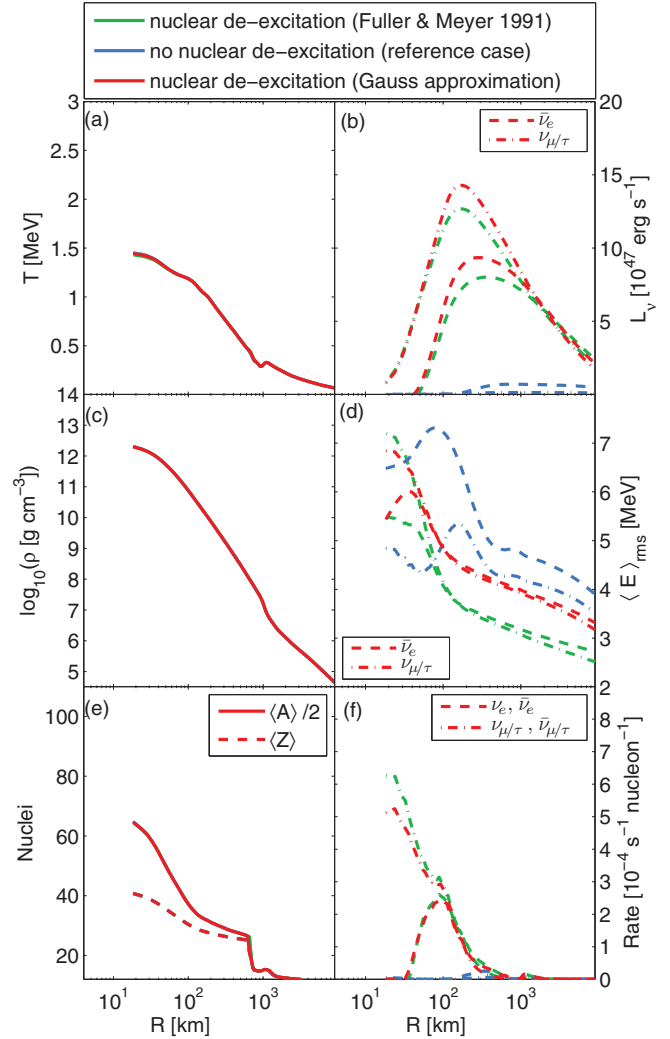


FIG. 6. (Color online) The same configuration as Fig. 5 but at about 3.5 ms before core bounce.

those for the de-excitation process. This is confirmed in Fig. 4, which shows that the luminosities of electron neutrinos, arising mainly from electron capture, are about 4 orders of magnitude larger than those of heavy-flavor neutrinos during the collapse phase.

We also find in Fig. 4 that the evolution of the  $\nu_e$  luminosities and RMS average energies are the same in all three simulations: the luminosity increases from about  $10^{51}$  to  $10^{53} \text{ erg s}^{-1}$  at  $\nu_e$  trapping shortly before core bounce caused by the increasing density which increases the electron Fermi energy and the capture rates. Relatedly, the RMS average energies of  $\nu_e$  increase from 6 MeV to 10 MeV. Note that these energies are much lower than those of the neutrinos directly produced by electron capture (see Fig. 3), reflecting the importance of down-scattering by interaction with matter.

There is, however, an important difference between electron capture and neutrino-pair heavy-nuclei de-excitation which becomes noticeable during collapse. The latter produces all neutrino types, while electron capture is a pure source of electron neutrinos. Indeed, we find that the de-excitation process is the dominating source of heavy-lepton-flavor neutrinos and,

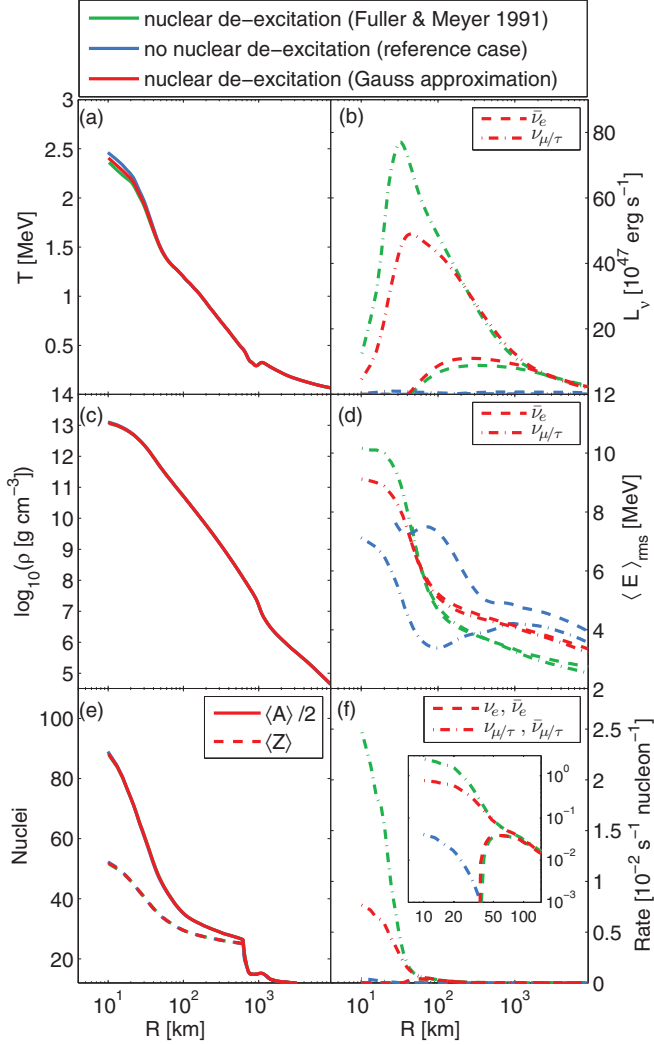


FIG. 7. (Color online) The same configuration as Figs. 5 and 6 but at about 1.5 ms before core bounce.

to a lesser extent, of electron antineutrinos during the collapse. At high densities of order  $10^{13} \text{ g cm}^{-3}$  also nucleon-nucleon bremsstrahlung becomes a source of neutrinos other than  $\nu_e$ . This process is also included in our control simulation and it is clearly visible in Fig. 4 by the steep rise of the  $\nu_{\mu,\tau}$  and  $\bar{\nu}_e$  luminosities at times of 1 ms just before bounce. In the early phase of the collapse, i.e., at lower temperatures and densities, neutrino-pair production by electron-positron annihilation is the dominating source of  $\bar{\nu}_e$  and  $\nu_{\mu,\tau}$ , where, due to the charge-current contribution, the  $\bar{\nu}_e$  luminosity is larger than for the heavy neutrino flavors. As can be seen in Fig. 3 neutrino-pair heavy-nuclei de-excitation becomes the dominating process for the production of heavy-flavor neutrinos and electron antineutrinos. We find rather similar  $\nu_{\mu,\tau}$  luminosities during this period for the two different approaches considered: in either case the luminosity increases from about  $10^{47}$  up to  $10^{49} \text{ erg s}^{-1}$ . During the same collapse phase the average energies of the heavy-flavor neutrinos increase slightly; however, their  $\langle E \rangle_{\text{rms}} \approx 2.2\text{--}3.5 \text{ MeV}$  values are noticeably smaller than the average energies of  $\nu_e$  neutrinos. (They are also smaller than the average neutrino energies produced in  $e^+e^-$

annihilation, which is the only heavy-lepton-flavor production mechanism in our reference simulation; see the discussion below.) As already noted above, we find slightly larger average energies when using the Gaussian model for the strength function than for the Fuller and Meyer approach. In either case, these values are equivalent to the free-streaming values listed in Table II for core temperatures below  $\sim 1 \text{ MeV}$ , which is the case until about 10 ms before core bounce. Only slightly before bounce when temperatures in excess of about 1 MeV (and  $\rho > 5 \times 10^{11} \text{ g cm}^{-3}$ ) are reached do the average energies start to rise significantly and their values begin to differ from the free-streaming values. This points to the relevance of neutrino-matter interactions also for heavy-flavor neutrinos.

At core bounce where normal nuclear matter density is reached, heavy nuclei dissociate into a state of homogeneous matter of nucleons and hence the production of neutrino pairs from nuclear de-excitation disappears. At shock formation and during the initial shock propagation out of the stellar core, the infalling heavy nuclei that hit the expanding shock wave also dissociate. Consequently, at the conditions behind the expanding shock front, weak processes are determined by interactions with free neutrons and protons. Hence, the inclusion of heavy-nuclei de-excitations has no impact on the supernova dynamics or the neutrino signal after core bounce, e.g., in terms of the energy loss such as suggested in Ref. [8]. Although a small fraction of heavy nuclei exist ahead of the expanding bounce shock before being dissociated, the conditions are such that other pair processes dominate over the pair production from nuclear de-excitation. Moreover, the supernova dynamics is dominated by charged-current processes on free nucleons behind the bounce shock in the dissociated regime. Consequently, neutrino-pair heavy-nuclei de-excitations has no impact in the entire post-bounce period and the evolution of the neutrino luminosities and average energies in our three simulation become identical.

Figures 5–7 show core profiles of important global quantities such as temperature, density, and the mean values for the charge  $\langle Z \rangle$  and mass number  $\langle A \rangle$  of the nuclear composition at selected snapshots during the collapse. Additionally, we have plotted the luminosities and average energies of the various neutrino types and the total rates of all neutrino-pair-production processes [processes (7)–(9) in Table I and nuclear de-excitation] which are relevant for the production of heavy-flavor neutrinos and electron antineutrinos during the collapse. Figures 5 and 6 reflect situations before and after onset of (electron) neutrino trapping in the core with central densities  $\lesssim 10^{11} \text{ g cm}^{-3}$  and a few times  $10^{12} \text{ g cm}^{-3}$ , respectively. Figure 7 shows profiles close to core bounce when the central density has reached values of a few times  $10^{13} \text{ g cm}^{-3}$ .

As our calculations involve dynamically adapting grids, comparisons between the three calculations with and without consideration of nuclear de-excitation are not straightforward. We have chosen the snapshots from our three simulations to match the core density profile. We then find that the profiles of the global quantities ( $T$ ,  $\rho$ ,  $\langle Z \rangle$ ,  $\langle A \rangle$ ) are the same, independent of whether or not nuclear de-excitation is considered in the simulation, again confirming that this neutrino-pair process has no influence on the supernova dynamics. Note the slight

mismatches in the central quantities, which are due to the imperfect matching of the evolutionary stages of the different simulations. We further observe from the snapshot figures that, due to electron captures on nuclei, the nuclear composition is shifted to more massive nuclei with larger neutron excess with progressing collapse. We have used this fact already to explain the differences in the rates and spectra calculated for the two nuclear de-excitation models considered in our simulation.

In our control study, without consideration of nuclear de-excitation,  $\bar{\nu}_e$  and  $\nu_{\mu,\tau}$  are produced by electron-positron annihilation and, at the high densities reached just before bounce in the center, by nucleon-nucleon bremsstrahlung (see Fig. 4). In Fig. 5 we observe that the electron-positron annihilation rate is restricted to the density regime roughly between  $10^6$  and  $10^{10} \text{ g cm}^{-3}$ . In this regime the rate is proportional to the product of the number densities of electrons and positrons,  $n_e n_{e^+} \sim \mu_e^3 T^3 \exp(-\mu_e/T)$ . Because the electron chemical potential  $\mu_e$ , which is roughly proportional to the third root of the density, grows faster during the collapse than the temperature, the exponential factor throttles the pair production by  $e^+e^-$  annihilation. Due to the charged-current contribution the production rate of electron neutrino pairs is larger than that of the other two flavors. Below  $10^{10} \text{ g cm}^{-3}$ , nuclear de-excitation increases the production rate of neutrino pairs, where the relative importance is larger for the heavy-flavor neutrinos than for electron neutrinos, due to the larger  $e^+e^-$  production rate of the latter. For densities in excess of  $10^{10} \text{ g cm}^{-3}$  the production of heavy-flavor and electron antineutrinos is basically only due to nuclear de-excitation. The pattern of the rate follows closely the one of temperature (the relevant parameter for the nuclear de-excitation rate, which is proportional to  $T^6$ ). The decrease of temperature toward the center is a consequence of the cooling by weak processes and it is the origin of the associated decrease of the de-excitation rate. The average neutrino energies produced by electron-positron annihilation shows a strong increase by about 1 MeV at a core radius of a few hundred kilometers. This rise correlates with the strong change in temperature. However, in this range the  $e^+e^-$  rate is strongly suppressed by the exponential factor, and neutrinos produced by nuclear de-excitation dominate. These neutrinos have smaller average energies than those produced by  $e^+e^-$  annihilation. As a consequence, the average neutrino energies calculated in our simulations with the inclusion of nuclear de-excitation are noticeable smaller than those found in the control calculation. Consistent with the discussion presented in Sec. III, we find that the nuclear de-excitation rate is larger using the model of Fuller and Meyer than using the Gauss approximation model, while the average neutrino energies are smaller.

Figure 6 shows a snapshot of the core profiles after onset of electron neutrino trapping in the center. Also under these conditions electron-positron annihilation and nuclear de-excitation are the two important neutrino-pair-production processes. Because, however, the temperature has risen significantly in the inner part (less than  $\sim 500$  km), the relative weight of the two processes has changed significantly due to their different dependence on temperature. While pair production from  $e^+e^-$  annihilation still occurs at distances of order 1000 km (where the temperature has not noticeably changed),

the temperature rise further inside causes an increase of the nuclear de-excitation rate by more than an order of magnitude. (Note the change of scales between Figs. 5 and 6.) This makes  $e^+e^-$  negligible for the determination of the spectra of neutrinos emitted from the core and as a consequence the average energies of the emitted  $\bar{\nu}_e$  and  $\nu_{\mu,\tau}$  became almost identical around 10 ms before bounce (see Fig. 4). In particular, the rate for production of heavy-flavor neutrinos follows the temperature profile and increases continuously toward the center. This is not the case for electron antineutrinos, where the trapping of electron neutrinos at densities in excess of about  $10^{11} \text{ g cm}^{-3}$  hinders the production of  $\nu_e \bar{\nu}_e$  pairs. The trapping also affects the spectra of  $\bar{\nu}_e$ . The presence of trapped electron neutrinos favors the production of  $\nu_e \bar{\nu}_e$  pairs with low-energy antineutrinos. Hence the respective average energies of  $\bar{\nu}_e$  are lower than for heavy-flavor neutrinos at the high energies where electron neutrinos are trapped. At lower densities the different neutrino types have quite similar average neutrino energies, reflecting the fact that nuclear de-excitation dominates as a neutrino-pair-production source. Comparing the results obtained from the two different approaches describing nuclear de-excitation, we find that the Gaussian approximation implies slightly larger average neutrino energies than the Fuller-Meyer ansatz, except at the highest temperatures and densities where the tail in the neutrino spectrum, as visible in the middle panel of Fig. 3, leads to a stronger increase of the average neutrino energies using the Fuller-Meyer approach. Note that, although the nuclear de-excitation rate increases toward the higher densities in the center, neutrino-matter interactions affect the transport of heavy-lepton-flavor neutrinos at densities in excess of a few times  $10^{11} \text{ g cm}^{-3}$  (see the decreasing average energies toward lower densities in Fig. 6). As a consequence, the average energies of the neutrinos emitted from the core (see Fig. 4) are substantially lower than the energy of neutrinos produced in the center.

Snapshots of the core profiles before bounce are shown in Fig. 7. The striking feature here, compared to the other two snapshots presenting earlier collapse phases, is the strong increase of temperature in the inner center at radii less than about 50 km, where the densities exceed  $10^{12} \text{ g cm}^{-3}$ . At these densities nucleon-nucleon bremsstrahlung contributes to the production of neutrino pairs, leading to a sizable increase in the production rate of heavy-flavor neutrinos in the control simulation (see the inset in the lower right panel of Fig. 7). Nevertheless, the high temperatures accelerate the production rate of heavy-flavor neutrinos by nuclear de-excitation which dominates over the  $N-N$  bremsstrahlung rate by more than an order of magnitude in this inner core. The inset also clearly demonstrates the suppression of electron-neutrino-pair production in the density range where electron neutrinos are trapped. As discussed above, neutrino matter interactions affect the neutrino transport in the high-density regime, causing the peak in the luminosity of heavy-flavor neutrinos and producing a drop in the average neutrino energies with increasing radius as neutrinos are down-scattered by scattering with electrons. Finally, we observe that the nuclear de-excitation rate obtained for the Fuller-Meyer approach is noticeably larger than for the Gauss approximation, which is

related to the assumed  $\langle A \rangle$  dependence of the former rate and its stronger contribution of forbidden strength.

We mention that inelastic neutrino scattering off nuclei, which is not included in our simulations, might contribute to the thermalization of neutrinos [4]. For  $\nu_e$  this process increases the energy exchange with matter by about 30%. As heavy-flavor neutrino scattering on electrons can only occur via neutral currents, i.e., in the absence of the exchange term present for electron neutrinos, the relative contribution of inelastic neutrino scattering on nuclei is expected to be larger than for electron neutrinos.

Can the neutrinos produced by nuclear de-excitation be observed by neutrino detectors? As discussed above, this process is the main source of  $(\mu, \tau)$  (anti)neutrinos during collapse. However, the associated neutrino energies are low so that neutral-current reactions are the only means to detect these neutrino flavors by earthbound detectors. Moreover, as the luminosity of  $\nu_e$  produced by electron capture is several orders of magnitude larger, experimental identification of  $(\mu, \tau)$  (anti)neutrinos seems impossible. This argument is strengthened by the fact that the  $\nu_e$  average energies are also significantly higher than those of  $(\mu, \tau)$  (anti)neutrinos, prohibiting an experimental identification above a certain energy cut. In contrast to the core-collapse phase, this appears to be possible during the cooling of the protoneutron star, where heavy-lepton-flavor neutrinos have generally higher average energies than  $\nu_e$ . The low luminosity and average energy of  $\bar{\nu}_e$  and  $(\mu, \tau)$  (anti)neutrinos produced by nuclear de-excitation will most likely prevent direct observation. However, the situation might be different if, in case of (complete) neutrino oscillations,  $\nu_e$  and  $\nu_{\mu,\tau}$  neutrinos swap their spectra [54]. In such a case an observation of “ $\nu_{\mu,\tau}$ ” neutrinos might become possible based on charged-current reactions as detection tools.

## V. SUMMARY AND CONCLUSIONS

The emission of neutrino pairs from the de-excitation of highly excited states in heavy nuclei had been proposed as a potential additional cooling source for core-collapse supernovae. We have tested this suggestion by performing supernova simulations which consider neutrino-pair nuclear de-excitation. In this article, we discussed this novel process based on two different approaches. First, we adopted the ansatz put forward by Fuller and Meyer [8] in which the relevant de-excitation strength function is described on the basis of the Fermi-gas model of independent nucleons. In a second approach, we have derived the de-excitation strength function from the inverse absorption process by exploiting the principle of detailed balance and describing the absorption strength function in a parametrized form guided by experimental data. These two choices of strength functions are quite distinct in their predictions about the importance of forbidden contributions to the strength, the energy centroids of the allowed and forbidden contributions, and the dependence of the total strength on details of the nuclear composition. However, when incorporated in the derivation of the neutrino-pair nuclear de-excitation rate, both approaches lead to qualitative similar results.

Contrarily to previous expectations, we find that nuclear de-excitation has basically no impact on the global supernova properties. In particular, this novel weak process leaves no imprint on the dynamics of the entire core-collapse supernova evolution up to several 100 ms post bounce. To this end, we have performed supernova simulations in spherical symmetry based on general relativistic radiation hydrodynamics and three-flavor Boltzmann neutrino transport, including nuclear de-excitation for both different approaches of the strength function. Compared to a reference simulation, where only the standard set of weak rates is considered, no impact on the dynamical evolution, e.g., on temperature (and entropy), was found. We find that electron capture on nuclei remains to be the dominating source of energy loss through most of the infall epoch, however, producing only electron neutrinos.

On the other hand, nuclear de-excitation produces neutrino pairs of all flavors. As correctly pointed out by Fuller and Meyer [8], this process produces heavy-lepton-flavor neutrinos and electron antineutrinos during the collapse phase. In standard supernova simulations, the production of these neutrino pairs is governed mainly by electron-positron annihilation resulting in low luminosities during the contraction of the stellar core. Including nuclear de-excitation raises their luminosities significantly but they are still lower by several orders of magnitude than the one for electron neutrinos produced by electron capture. This is related to the significantly smaller pair-production rates from nuclear de-excitation, compared to electron captures, for most of the core-collapse phase. Only a few milliseconds before core bounce, when the matter temperatures reach 3–5 MeV, does the strong  $T$  dependence of nuclear de-excitation lead to a strong rise of the local pair-production rate. Moreover, the locally produced neutrinos from nuclear de-excitation, in particular  $(\nu_{\mu,\tau})$ , interact noticeably with matter. These mainly entail inelastic scattering on electrons (and potentially inelastic scattering with nuclei, which has not been considered in our simulations). It makes the proper treatment of neutrino transport also essential for heavy-flavor neutrinos during the core-collapse phase. As a result of the interactions with matter, heavy-flavor neutrinos produced at sufficiently high densities thermalize their spectra, similarly to  $\nu_e$  neutrinos, until they can escape the collapsing stellar core. They have lower average energies than electron neutrinos, which, together with their significantly lower luminosities, makes their detection in the absence of neutrino-flavor oscillation scenarios very difficult.

We mention that in the present simulations inelastic neutrino scattering off nuclei is not included. In Ref. [4] it has been argued that for  $\nu_e$  this process increases the energy exchange with matter by about 30%. For  $(\mu, \nu)$  (anti)neutrinos the relevance of inelastic neutrino-nucleus scattering might be larger, given that the rate for inelastic neutrino scattering on electrons is noticeably smaller for heavy-flavor neutrinos than for electron neutrinos, while the inelastic neutrino-nucleus scattering rate is the same for all flavor types.

Electron neutrinos start to become trapped at densities of around  $10^{11} \text{ g cm}^{-3}$ , above which also the production of  $\bar{\nu}_e$  from heavy-nuclei de-excitation is seen. Such densities are reached only very shortly (a few milliseconds) before core bounce. Hence the time scale for the continued production

of heavy-lepton-flavor neutrinos, which are not trapped, is not efficient enough to impact the very final evolution until core bounce. At densities of a few times  $10^{13}$  g cm $^{-3}$ , which corresponds to temperatures of roughly 4 MeV, other neutrino-pair processes such as nucleon-nucleon bremsstrahlung starts to contribute besides nuclear de-excitation. They produce neutrinos at significantly higher energies and at higher luminosity. At even higher temperatures, when the core reaches correspondingly nuclear matter densities and where heavy nuclei dissolve, weak processes with free nucleons dominate. In particular, neutrino pairs are no longer being produced by nuclear de-excitation. This holds for the entire post-bounce phase, which is dominated by mass accretion prior to the possible onset of an explosion, where temperatures and entropies behind the bounce shock are so high that heavy nuclei cannot exist.

Note that the nuclear description applied here to deduce reaction rates for the de-excitation of heavy nuclei by the

emission of neutrino pairs is rather crude. Nevertheless, we do not expect that an improved treatment of nuclear structure relevant for this weak-interaction process will significantly alter our conclusions.

## ACKNOWLEDGMENTS

The supernova simulations were performed at the computer center of the GSI, Helmholtzzentrum für Schwerionenforschung GmbH, in Darmstadt, Germany. TF is supported by the Narodowe Centrum Nauki (NCN) within the “Maestro” program under Contract No. DEC-2011/02/A/ST2/00306. GMP is partly supported by the Deutsche Forschungsgemeinschaft through Contract No. SFB 634, the Helmholtz International Center for FAIR within the framework of the LOEWE program launched by the state of Hesse, and the Helmholtz Association through the Nuclear Astrophysics Virtual Institute (VH-VI-417).

- 
- [1] H. A. Bethe, *Rev. Mod. Phys.* **62**, 801 (1990).
  - [2] H.-T. Janka, K. Langanke, A. Marek, G. Martínez-Pinedo, and B. Müller, *Phys. Rep.* **442**, 38 (2007).
  - [3] S. Woosley, A. Heger, and T. Weaver, *Rev. Mod. Phys.* **74**, 1015 (2002).
  - [4] K. Langanke, G. Martínez-Pinedo, B. Muller, H.-T. Janka, A. Marek, W. R. Hix, A. Juodagalvis, and J. M. Sampaio, *Phys. Rev. Lett.* **100**, 011101 (2008).
  - [5] H. A. Bethe, G. E. Brown, J. Applegate, and J. M. Lattimer, *Nucl. Phys. A* **324**, 487 (1979).
  - [6] K. Langanke and G. Martínez-Pinedo, *Rev. Mod. Phys.* **75**, 819 (2003).
  - [7] R. Buras, H.-T. Janka, M. T. Keil, G. G. Raffelt, and M. Rampp, *Astrophys. J.* **587**, 320 (2003).
  - [8] G. M. Fuller and B. S. Meyer, *Astrophys. J.* **376**, 701 (1991).
  - [9] M. Liebendörfer *et al.*, *Astrophys. J. Suppl.* **150**, 263 (2004).
  - [10] G. W. Misch, B. A. Brown, and G. M. Fuller, *Phys. Rev. C* **88**, 015807 (2013).
  - [11] D. M. Brink, *Proc. Phys. Soc. A* **68**, 994 (1955).
  - [12] S. W. Bruenn, *Astrophys. J. Suppl.* **58**, 771 (1985).
  - [13] S. Reddy, M. Prakash, and J. M. Lattimer, *Phys. Rev. D* **58**, 013009 (1998).
  - [14] A. Juodagalvis, K. Langanke, W. R. Hix, G. Martínez-Pinedo, and J. M. Sampaio, *Nucl. Phys. A* **848**, 454 (2010).
  - [15] A. Mezzacappa and S. Bruenn, *Astrophys. J.* **405**, 637 (1993).
  - [16] A. Mezzacappa and S. Bruenn, *Astrophys. J.* **410**, 740 (1993).
  - [17] S. Hannestad and G. Raffelt, *Astrophys. J.* **507**, 339 (1998).
  - [18] G. G. Raffelt, *Astrophys. J.* **561**, 890 (2001).
  - [19] M. T. Keil, G. G. Raffelt, and H.-T. Janka, *Astrophys. J.* **590**, 971 (2003).
  - [20] T. Fischer, G. Martínez-Pinedo, M. Hempel, and M. Liebendörfer, *Phys. Rev. D* **85**, 083003 (2012).
  - [21] J. M. Lattimer and F. Swesty, *Nucl. Phys. A* **535**, 331 (1991).
  - [22] H. Shen, H. Toki, K. Oyamatsu, and K. Sumiyoshi, *Nucl. Phys. A* **637**, 435 (1998).
  - [23] M. Hempel and J. Schaffner-Bielich, *Nucl. Phys. A* **837**, 210 (2010).
  - [24] M. Hempel, T. Fischer, J. Schaffner-Bielich, and M. Liebendörfer, *Astrophys. J.* **748**, 70 (2012).
  - [25] A. W. Steiner, M. Hempel, and T. Fischer, *Astrophys. J.* **774**, 17 (2013).
  - [26] F. X. Timmes and D. Arnett, *Astrophys. J. Suppl.* **125**, 277 (1999).
  - [27] A. L. Cole, T. S. Anderson, R. G. T. Zegers, S. M. Austin, B. A. Brown, L. Valdez, S. Gupta, G. W. Hitt, and O. Fawwaz, *Phys. Rev. C* **86**, 015809 (2012).
  - [28] S. E. Koonin, D. J. Dean, and K. Langanke, *Phys. Rep.* **278**, 2 (1997).
  - [29] K. Langanke *et al.*, *Phys. Rev. Lett.* **90**, 241102 (2003).
  - [30] W. R. Hix, O. E. B. Messer, A. Mezzacappa, M. Liebendörfer, J. Sampaio, K. Langanke, D. J. Dean, and G. Martínez-Pinedo, *Phys. Rev. Lett.* **91**, 201102 (2003).
  - [31] K. Langanke, E. Kolbe, and D. J. Dean, *Phys. Rev. C* **63**, 032801 (2001).
  - [32] T. D. Thomas, *Nucl. Phys.* **53**, 558 (1964).
  - [33] T. D. Thomas, *Annu. Rev. Nucl. Sci.* **18**, 343 (1968).
  - [34] J. R. Grover and J. Gilat, *Phys. Rev.* **157**, 802 (1967).
  - [35] R. Capote *et al.*, *Nucl. Data Sheets* **110**, 3107 (2009).
  - [36] M. Rampp and H.-T. Janka, *Astron. Astrophys.* **396**, 361 (2002).
  - [37] F. Osterfeld, *Rev. Mod. Phys.* **64**, 491 (1992).
  - [38] O. Hausser, *Can. J. Phys.* **65**, 691 (1987).
  - [39] M. Uchida *et al.*, *Phys. Lett. B* **557**, 12 (2003).
  - [40] B. D. Anderson, N. Tamimi, A. R. Baldwin, M. Elaasar, R. Madey, D. M. Manley, M. Mostajabodda'vati, J. W. Watson, W. M. Zhang, and C. C. Foster, *Phys. Rev. C* **43**, 50 (1991).
  - [41] M. Sasano *et al.*, *Phys. Rev. Lett.* **107**, 202501 (2011).
  - [42] K. Heyde, P. von Neumann-Cosel, and A. Richter, *Rev. Mod. Phys.* **82**, 2365 (2010).
  - [43] E. Caurier, G. Martínez-Pinedo, F. Nowacki, A. Poves, and A. P. Zuker, *Rev. Mod. Phys.* **77**, 427 (2005).
  - [44] E. Kolbe, K. Langanke, G. Martínez-Pinedo, and P. Vogel, *J. Phys. G* **29**, 2569 (2003).
  - [45] W. C. Haxton, K. Langanke, Y.-Z. Qian, and P. Vogel, *Phys. Rev. Lett.* **78**, 2694 (1997).
  - [46] Y.-Z. Qian, W. C. Haxton, K. Langanke, and P. Vogel, *Phys. Rev. C* **55**, 1532 (1997).
  - [47] E. Litvinova, H. P. Loens, K. Langanke, G. Martínez-Pinedo, T. Rauscher, P. Ring, F.-K. Thielemann, and V. Tselyaev, *Nucl. Phys. A* **823**, 26 (2009).

- [48] K. Langanke, G. Martínez-Pinedo, P. von Neumann-Cosel, and A. Richter, *Phys. Rev. Lett.* **93**, 202501 (2004).
- [49] R. W. Fearick, G. Hartung, K. Langanke, G. Martínez-Pinedo, P. von Neumann-Cosel, and A. Richter, *Nucl. Phys. A* **727**, 41 (2003).
- [50] A. Juodagalvis, K. Langanke, G. Martínez-Pinedo, W. R. Hix, D. J. Dean, and J. M. Sampaio, *Nucl. Phys. A* **747**, 87 (2005).
- [51] E. Kolbe and K. Langanke, *Phys. Rev. C* **63**, 025802 (2001).
- [52] K. Langanke and G. Martínez-Pinedo, *Nucl. Phys. A* **673**, 481 (2000).
- [53] K. Langanke, G. Martínez-Pinedo, and J. M. Sampaio, *Phys. Rev. C* **64**, 055801 (2001).
- [54] H. Duan, G. M. Fuller, and Y.-Z. Qian, *Annu. Rev. Nucl. Part. Sci.* **60**, 569 (2010).